CORA Cork Open Research Archive
Cartlann Taighde Oscailte Chorcaí

Title	Dissociative adsorption of methane on the Cu and Zn doped (111) surface of CeO2
Authors	Carey, John J.;Nolan, Michael
Publication date	2016-04-04
Original Citation	Carey, J. J. and Nolan, M. (2016) 'Dissociative adsorption of methane on the Cu and Zn doped (111) surface of CeO2', Applied Catalysis B: Environmental, 197, pp. 324-336. doi: 10.1016/j.apcatb.2016.04.004
Type of publication	Article (peer-reviewed)
Link to publisher's version	10.1016/j.apcatb.2016.04.004
Rights	© 2016, Elsevier B.V. This manuscript version is made available under the CC-BY-NC-ND 4.0 license https://creativecommons.org/licenses/by-nc-nd/4.0/ - https://creativecommons.org/licenses/by-nc-nd/4.0/
Download date	2026-11-06 15:26:30
Item downloaded from	https://hdl.handle.net/10468/3199

UCC
University College Cork, Ireland
Coláiste na hOllscoile Corcaigh

Dissociative adsorption of methane on the Cu and Zn doped (111) surface of CeO_2

John J. Carey[†*] and Michael Nolan[†*]

[†]Tyndall National Institute, University College Cork, Lee Maltings, Dyke Parade, Cork, Ireland

KEYWORDS Methane activation, density functional theory, CeO_2, transition metal doping,

ABSTRACT: The development of economical heterogeneous catalysts for the activation of methane is a major challenge for the chemical industry. Screening potential candidates becomes more feasible using rational catalyst design to understand the activity of potential catalysts for CH_4 activation. The focus of the present paper is the use of density functional theory to examine and elucidate the properties of doped CeO_2. We dope with Cu and Zn transition metals having variable oxidation state (Cu), and a single oxidation state (Zn), and study the activation of methane. Zn is a divalent dopant and Cu can have a +1 or +2 oxidation state. Both Cu and Zn dopants have an oxidation state of +2 after incorporation into the CeO_2 (111) surface; however a Hubbard +U correction (+U=7) on the Cu 3d states is required to maintain this oxidation state when the surface interacts with adsorbed species. Dissociation of methane is found to occur locally at the dopant cations, and is thermodynamically and kinetically more favorable on Zn-doped CeO_2 than Cu-doped CeO_2. The origins of this lie with the Zn(II) dopant moving towards a square pyramidal geometry in the sub surface layer which facilitates the formation of two-coordinated surface oxygen atoms, that are more beneficial for methane activation on a reducible oxide surface. These findings can aid in rational experimental catalyst design for further exploration in methane activation processes.

1. Introduction

Methane derived from biodegradable matter (biomass) has great potential as a renewable carbon source for a range of applications such as syngas,[1] methanol,[2] formaldehyde,[3] and biofuel production.[4] The main issue associated with utilization of methane is the CH bond activation process, which has a large associated energy cost of 440 kJ/mol to dissociate the first CH bond of CH_4 to CH_3^* +H.[5] A catalyst is therefore required to lower the energy cost and improve the bond dissociation process for more efficient exploitation of methane gas. Extensive investigations of methane activation on the transition metal surfaces of Ni, Pt, Rh, Ir, Pd, and Ru have revealed that Pt, Rh and Ir show the most promising behavior to promote efficient methane activation.[6-8] The associated high cost of these metals however, is problematic for economic implementation as heterogeneous catalysts in the petrochemical industry. In addition these metal surfaces are selectively poisoned over time by carbonaceous deposits from successive dehydrogenation of adsorbed CH_x species (x=1-3), and oxygen ad-atoms from atmospheric O_2, eventually rendering the catalyst inactive.[9] This is a major problem in the use of transition metal catalysts for CH_4 activation, and therefore alternative, economical candidates but with a similar reactivity are desired.

The use of a metal oxide as a support for highly dispersed transition metals improves resistivity to carbon poisoning, as the lattice oxygen from the support was found to interact with the carbonaceous deposits to form CO and CO_2.[10] The reducibility of the support can therefore play a role in removing the carbon deposits from the transition metal clusters as the more easily reducible the metal oxide surface, the more mobile the oxygen species are for interacting with the carbon atoms.[10, 11] Investigations into the role of the metal oxide support on the removal of carbonaceous deposits by lattice oxygen found that the catalyst is regenerated after CO_x formation for further decomposition of methane, outlining the im-

portance of using a reducible oxide in the catalyst bed.[12, 13] The hydrogen atoms produced during the successive dehydrogenation of the CH_x (x=1-3) species during the reaction were found to either form H_2 gas and/or interact with lattice oxygen or atmospheric oxygen to form H_2O.[14] The formation of CO and H_2 from CH_4 activation is typical for syngas production and highly desirable;[1] however thermodynamic selectivity towards CO_2 and H_2O as products is unwanted due to the low reactivity of these molecules. Transition metals supported on oxides were found to be reactive for the activation of the CH_4, and in some cases more reactive than the single transition metal clusters as seen for Pd and PdO,[15] indicating that the support does not hinder the catalytic process. The use of transition metals in these catalysts however, still has a large associated cost, and development of inexpensive precious metal free catalysts that are resistant to carbon and oxygen poisoning, while maintaining a high reactivity towards methane activation, are highly desirable.

Reducible metal oxide catalysts are potential methane activation catalysts and there is a strong focus on improving their properties to carry out this process more efficiently.[16] The role of lattice oxygen is found to be important for oxygenation reactions and thus can be useful to facilitate the partial oxidation of methane (POM) to selectively produce syngas.[17-19] POM on reducible oxide catalysts has also been investigated for the production of methanol, formaldehyde and other useful oxygenate carbon species for renewable energy applications. One particular potential candidate for this process is cerium dioxide (CeO_2) since it is a highly reducible metal oxide and exhibits favorable reactivity for methane activation.[13] The presence of Ce as a non-native dopant in other transition metal supported oxide systems was also found to have a promoting effect on the POM reaction to produce highly desirable syngas indicating that Ce plays an important role for this reaction process.[12] The incorporation of Pt into the CeO_2 lattice was found to improve the catalyst performance for methane activation, as the transition metal dopant cation enhances the formation of oxygen vacancies and thus the oxygen mobility within the CeO_2 lattice, which improves the POM reaction process.[12, 20] This suggests that there is a correlation between

the reducibility of the metal oxide and methane activation, and therefore improving the reducibility of the metal oxide can increase the activity for methane activation.

The activation of methane was investigated by density functional theory (DFT) calculations on the bare, Zr and Pd doped (111) surface of CeO_2.[21] The presence of the dopant reduced the kinetic barriers for activating the CH bond from 1.40eV (pure) to 1.06eV (Zr doped) and 0.22eV (Pd doped); however Pd being a divalent dopant should have a compensating oxygen vacancy in the CeO_2 surface for a correct ground state electronic structure,[22] which is not considered in ref,[21] thus producing questionable results. The reduced barriers indicate that methane activation is greatly improved compared to the pure CeO_2 (111) surface through the introduction of dopants. The enhanced POM process for Pd based oxides has been investigated by experiment and DFT studies which have attributed the greater activation to the active PdO phase in its native oxide.[15] The metal and metal oxide interaction having an improved performance for methane dissociation suggests that transition metals that form binary oxides such as PdO may be strong potential candidates for the POM process, as they can form M-O bonds in the catalyst, which may offer an explanation for Pt also improving methane activation in CeO_2 catalysts.[10, 12] To understand the role of doping the CeO_2 lattice with transition metals to activate methane, DFT calculations have developed a relationship between bond activation energies and adsorption energies of the dissociation products (CH_3^* + H).[23] The calculations found that a linear relationship exists between the adsorption energy and the activation energy, with the stronger binding having a lower activation barrier. A correlation between oxygen vacancy formation and methane activation was also determined; dopants with smaller oxygen vacancy formation energies have a higher affinity to methane activation. The choice of dopants to examine for methane activation was thus based on candidates with low oxygen vacancy formation energies, as these are; Zn, Ni, Ag, Pt, Mn, V, Pd, Zr and W. Among these dopants, the highest activation energy was associated with the dopant that had the lowest adsorption energy of the dissociated products. From these studies there are two factors that are found to govern the properties of

a doped CeO_2 surface; (1) the oxygen vacancy formation energy of the dopant, and (2) the stability of the dissociated products. Examination of these quantities is important for the choice of dopant species to promote methane activation on the CeO_2 surface.

Closer examination of DFT studies for methane activation on CeO_2[21, 23] reveals some questions over the energies for the oxygen vacancy formation, C-H bond activation and methane dissociation. The oxygen vacancy formation energies for dopants with a +2 valance state in their host oxide are negative which indicates that oxygen vacancies will be present in the +2 doped CeO_2 lattice.[22] The adsorption energies for the methane dissociation products are also very stable on the +2 doped CeO_2 surfaces compared to the other doped surfaces in the study. The calculated activation energy for Zn. Mn and Ni doped CeO_2 appear to be close to or less than 0.00eV, which are questionable values since pseudo and real transition states are observed that may suggest complications in the approach to modelling the surfaces.[23] The problems outlined with previous works for methane activation can be attributed to the neglect of a charge compensated oxygen vacancy for a dopant species with an oxidation state of +2. Introduction of +2 dopants on the Ce^{4+} lattice site creates two holes (positive charge) on two neighboring oxygen atoms, that is, creating O^- species in the CeO_2 lattice. The presence of two O^- species requires the removal of an oxygen atom to balance the positive charge with two electrons from the creation of a neutral oxygen vacancy. This charge compensating vacancy conserves the overall charge of the system; otherwise the ground state electronic structure is incorrect and may provide questionable results for Cu^{2+}, Zn^{2+}, Mn^{2+} and other +2 dopants,[23] which are seen to have hole states on the oxygen atoms from spin density plots, but the reason for this is not addressed at all, and re-evaluation of the electronic structure and energetics for these dopants is needed. The importance of the charge compensating vacancy has therefore been overlooked in previous DFT studies on methane activation,[21, 23] which is surprising as the dissociation products are electron donating species that can fill the holes at the surface leading to overbinding, and thus stabilizing adsorption products and reducing kinetic energies. The importance of the

charge compensating vacancy has been shown for doping bulk CeO_2, CeO_2 (111) and (100) surfaces with transition metals and alkaline earth metals that have a valence state of +2, promoting the spontaneous oxygen vacancy formation through charge compensation.[22, 24, 25] The next oxygen is the vacancy for which the vacancy formation energy is relevant.[22]

Potential candidates to promote methane activation at the CeO_2 (111) surface through substitutional doping that exist in +2 oxidation states in their native oxides are Cu and Zn. These dopants have been shown to promote oxygen vacancy formation in the bulk CeO_2 lattice,[24] and may therefore improve surface oxygen vacancy formation and methane activation compared to undoped CeO_2. Cu^{2+} cations have been doped into CeO_2 to promote reactions including the steam reforming of methanol,[26] methanol synthesis,[27] CO oxidation,[28] SO_2 decomposition,[29] water-gas shift reaction,[30] nitrogen monoxide reduction,[31] and methanol synthesis from CO and H_2.[32] The incorporation of Cu in the CeO_2 lattice is therefore expect to promote reactions that are dependent on oxidation processes which includes the POM process; however to our knowledge the effect of Cu doping for methane activation on the CeO_2 (111) surface has not been addressed. Zn doped into the CeO_2 lattice seen to promote oxygen vacancy formation,[33] CO oxidation,[34] and Cu-Zn-CeO_2 catalysts have been examined for steam reforming of methanol,[35] and dimethyl ether[36].

The present paper presents a DFT+U study of the methane activation on the Cu and Zn doped (111) surface of CeO_2. The choice of Cu and Zn as dopant cations at the surface interface originates from these dopants having +2 oxidation states in their parent oxides. Dopants with this oxidation state will allow spontaneous oxygen vacancy formation potentially promoting oxygen mobility at the surface, which has been shown by both experiment and theory to be an important characteristic for POM catalysts.[20, 23] The inclusion of a charge compensating oxygen vacancy avoids inaccuracies for the adsorption of the dissociation products. As Cu can have two oxidations states as CuO and Cu_2O, thus having variable valence, while Zn only exists as ZnO, we will also examine the effect, if any, of dopant reduci-

bility in CeO_2 for POM. The effect of a Hubbard +U correction on the Cu and Zn 3d states is also investigated, by applying the PBE GAA, with a +U= 0eV (no correction) and U= 7 /7.8eV for Cu/Zn 3d states. The calculations will provide a valuable insight into the choice of dopant species for rational experimental catalyst design in the technologically significant methane activation process.

2. Computational Methods

All calculations were carried out using DFT and the generalized gradient (GGA) approximation, with the Perdew-Burke-Ernzerhof (PBE)[37] exchange-correlation functional as implemented in the Vienna *ab initio* Simulation Package (VASP).[38-41] The valence electrons (Cu[$3p^6$, $3d^{10}$, $4s^1$], Zn[$3d^{10}$, $4s^2$], C/O [$2s^2$, $2p^{3/4}$], Ce[$5s^2$ $5p^6$ $6s^2$ $5d^1$ $4f^1$]) were expanded using a plane wave basis set approach, while the interactions with the core electrons (C/O[He], Cu/Zn[Ar], Ce[Rn]) were described using the projector augmented wave (PAW) approach.[42] Non-spherical contributions from the gradient corrections inside the PAW radii are also included, which are important for accurate total energy calculations.

To correct for the strong electronic correlation with bulk CeO_2, the well-known PBE+U approach was used with a $+U$ parameter of 5eV applied to the Ce 4*f* states which is a commonly used value in many studies on CeO_2.[43-45] For Cu and Zn, the question of the value of U in a DFT+U approach needs to be considered. For Zn, including a +U or self-interaction correction on the 3d states can shift the position of these occupied states relative to the valence band.[46-48] We have checked the effect of a U value of 7.8 eV on the Zn 3d states[49] on the vacancy formation energies and the molecular adsorption energies and we find at most a change of 0.02 eV in these energies, with no change to the stable structures or oxidation states. This indicates that the effect of the +U correction on the Zn 3d states for the properties of interest in this paper is negligible.

For Cu, on the other hand, it is known that some sort of correction, whether DFT+U, Self-Interaction Corrected or hybrid DFT is needed to describe bulk CuO.[50-52] In ref.[50] a value of 7 eV was applied to

describe the Cu 3d states in bulk CuO and arrive at a band gap and magnetic moment that were consistent with experiment and earlier self-interaction corrected results.[51] Since the issues of describing bulk CuO with DFT involve all Cu atoms in the bulk we reasoned that for a single Cu dopant this would not necessarily be a significant issue. Our studies of Cu-doped CeO_2 (111) have been undertaken without a +U correction and with a +U correction applied to the Cu 3d states, setting U = 7 eV. The +U correction provides the correct description of the electronic structure for Cu-CeO_2. The inclusion of a +U correction to the Cu 3d states widens the energy gap between the occupied and unoccupied Cu 3d states which has its more pronounced implications when adsorbates are present on the surface. If no correction is applied the Cu dopant can oxidize to a +3 oxidation state upon H adsorption, which in these systems is not realistic. All Cu-CeO_2 calculations are therefore presented with a U = 7eV on the Cu 3d states; results for the Cu-CeO_2 surfaces without a +U correction (+U=0) are supplied in the supporting information to enable the interested reader to make a comparison between the two approaches

Finally, we do not apply any DFT+U correction to the oxygen atoms in doped CeO_2. The substitution of a Ce atom for a divalent cation introduces two holes as a result of the different oxidation state. In some systems, such as Li-doped MgO or Al-doped SiO_2, a +U correction to the O 2p states was needed to describe consistently the resulting hole localization.[53, 54] However, in the present case, along with our earlier work on divalent dopants in ceria,[55, 56] we find that oxygen vacancy compensation of the divalent dopant takes place and there are no issues over describing oxygen holes, as these are compensated by the electrons released by oxygen vacancy formation. Accordingly the ground state of divalent doped CeO_2 (111) is that in which an oxygen vacancy is present.

The technical parameters within all calculations are an energy cut-off of 400eV and a Monkhorst Pack *k*-point sampling grid of (4x4x4) for bulk and (1x2x1) for the (111) surface. A (111) surface was cut from the bulk structure, with a slab thickness of 9 atomic layers (3 O-Ce-O trilayers) extended in the *xy* plane and a vacuum gap of 15Å above the surface to remove any slab interactions in the *c* vector. The

bottom three atomic layers (tri-layer) were held fixed in the bulk lattice positions and the top six layers were allowed to fully relax. The surface was expanded to a *p*(4x2) structure and relaxed, where the *c*-vector did not require any additional sampling. Dopants were substituted for Ce cations at the surface lattice positions, giving a concentration of 4% and then the atomic positions were relaxed. The bulk, and all subsequent structures were optimized using the conjugant gradient method and deemed converged when the forces on the atoms were determined to be less than 0.02 eV/Å.

The position of the charge compensating vacancy was extensively explored in the surface and sub surface layers of the doped surfaces, with the oxygen vacancy formation energy being calculated by;

$$E_f\,[comp] = (E[comp] + \tfrac{1}{2}\,E[O_2]) - E[surf] \qquad (1)$$

Where E_f [comp] is the calculated formation energy for the compensating vacancy, E[comp] is the energy of the surface with the compensating vacancy, $E[O_2]$ is the energy for gas phase O_2 and E[surf] is the energy of the doped surface. The active vacancy was determined by examining the removal of the second oxygen atom in the compensated structure and the formation energy is calculated by;

$$E_f\,[active] = (E[active] + \tfrac{1}{2}\,E[O_2]) - E[comp] \qquad (2)$$

Where E_f [active] is the formation energy for the active vacancy, E[active] is the energy for the surface with the active vacancy, $E[O_2]$ is the energy for gaseous oxygen and E[comp] is the energy for the compensated structure. The energy of O_2 in the vacancy formation energies is computed using the PBE-GGA which is known to cause errors in the O_2 binding energy, around 0.7 eV.[57-60] Our values are therefore made more negative by 0.35eV (per atom) to include this error, however its inclusion will not affect any of the findings and trends in this paper.

The lowest energy configuration for each of the molecular and atomic adsorbate species on the doped surfaces were determined by examining all possible surface adsorption sites and calculating the adsorption energy for each species by the equation;

$$E[ads] = E[sys] - (E[comp] + E[gas]) \qquad (3)$$

Where E[ads] is the calculated adsorption energy, E[sys] is the energy for the adsorbate on the doped surface, E[comp] is the calculated energy for the compensated surface and E[gas] is the calculated energy of the molecule in the gas phase. Negative adsorption energies indicate that adsorption of the species is favorable; while a positive energy indicates that the adsorption is disfavored relative to the gas phase species. The electronic structure was analyzed using spin density plots, and partial (ion and *l* quantum number decompose) density of states (PEDOS). The charge analysis was carried out using Bader AIM approach,[61-63] and the activation energy barriers for CH bond breaking were determined using the climbing image nudged elastic band (CI-NEB) approach.[64, 65] The nature of the cNEB approach we applied is that it will explicitly find the highest energy point on the potential energy surface between the starting and end structures that anchor the calculation. A vibrational calculation is used to confirm that the obtained transition state is a true maximum on the potential energy surface since it has an imaginary frequency associated with a single vibrational mode. The CI-NEB calculations are carried out using a Newton-Raphson minimization method, and are deemed converged when the forces are less than 0.02eV/Å on Cu doped CeO_2, and 0.04eV/Å on Zn doped CeO_2 due to difficulties with convergence.

3. 3. Results

3.1 Bare and Reduced CeO_2 (111)

The (111) surface of CeO_2 is the most thermodynamically stable surface, and has received much attention in the literature. The structure of the pure CeO_2 (111) surface is well established, [43, 44] and will not be described in detail here. The relaxed surface and calculated PEDOS plots of the undoped CeO_2 (111) surface are shown in Figure 1. The CeO_2 (111) surface is oxygen terminated with Ce cations lying below, and the PEDOS shows that the surface valence band (VB) is dominated by O 2*p* states, while the lowest unoccupied states are the localised Ce 4*f* states with a VB to Ce 4*f* gap of 2.39eV.

The reducibility of the (111) surface is important to mention so that a comparison can be made to the doped surfaces in the following sections. The most favorable position of the oxygen vacancy is well known to be in the subsurface layer over the surface oxygen atoms,[43-45] with the oxygen vacancy reducing two Ce cations from Ce(IV) to Ce(III). A number of possible Ce(III) distributions can occur after oxygen vacancy formation that range in energy giving different energy solutions as a spread of 0.3 eV as a function of Ce(III) distributions.[66-68] The oxygen vacancy formation energy within our DFT+U set up is calculated to be 1.84eV, falling in an acceptable range for previously reported Ce(III) distributions, and can be used as a guideline for comparing to the oxygen vacancy formation in the doped surfaces.

The reduction of the Ce cations on the surface after oxygen vacancy formation, results in the presence of a Ce 4f defect peak in the band gap around 1.11eV between the top of the valence band (VB) and the unoccupied Ce 4f states. The Ce 4f defect peat is associated with the two electrons that are localized on two Ce(III) cations. Both electrons have up spin indicating that a ferromagnetic (FM) ground state electronic structure is preferred over an anti-ferromagnetic (AFM) for the reduced CeO2 (111) surface. The reduction of the Ce cations is confirmed by Bader charges which indicate a gain of 0.32 electrons compared to the bare CeO2 (111) surface. Spin magnetization values of 0.99 on each reduced Ce cation further supports this mechanism.

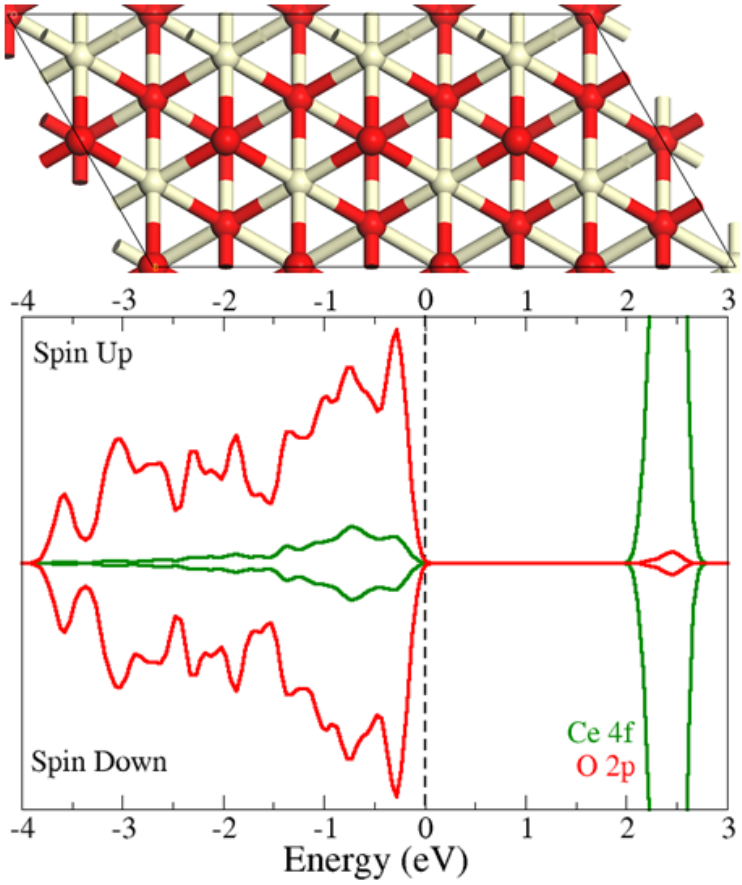


Figure 1: The calculated structure and PEDOS plots for the undoped (111) surface of CeO_2. The white and red spheres are the lattice positions of the Ce and O atoms. The red and green lines are the O 2*p* and Ce 4*f* contributions to the valence and conduction bands, with the top of the valence band being aligned to 0eV.

3.2 Cu and Zn doped CeO_2 (111)

The most favorable dopant position in the CeO_2 lattice was examined by substituting one Ce cation in the surface or sub-surface layers. For both Cu and Zn, the dopant prefers to substitute on a surface Ce site, which is shown in Figure 2. Upon relaxation, irrespective of whether a +U correction is applied or not, the Cu dopant undergoes significant migration off the Ce lattice site to form a square planar configuration in which it bonds to a surface oxygen (Cu-O distance of 1.90Å), two sub-surface oxygens in the

same plane as Cu (Cu-O distance 1.87x2) and an oxygen in the sub layer (Cu-O, 1.93Å) that is pulled out of this subsurface layer. The bonds above and below the dopant are longer than the bonds in the plane of the dopant, consistent with a Jahn-Teller distortion. The Cu^{+2} dopant with a d^9 configuration adopts this geometry to accommodate the extra electron in the high energy $dx^2 - y^2$ orbital, which is known for Cu^{+2} complexes,[69] bulk CuO and Cu doped bulk CeO_2.[24] The displacement of Cu distorts the local surface geometry, leaving two oxygen surface atoms with two-fold coordination and a three-coordinated sub-surface oxygen atom. This description of the local geometry around the Cu dopant and its electronic configuration is independent of the DFT approach used.

In contrast to Cu doped CeO_2, the most significant migration observed for the Zn dopant is a down-ward shift to the next sublayer by 0.55Å, giving the Zn dopant a four coordinate distorted tetrahedral geometry; Zn bonds to three sub-surface oxygen with Zn-O distances of 2.00Å, and to an oxygen atom in the sublayer below the dopant with a Zn-O distance of 2.08Å. This oxygen migrates from its lattice position towards the dopant. The presence of the Zn dopant in the surface creates three two-fold coordi-nated surface oxygen atoms, which bridge between Ce cations on the surface around the dopant.

Cu and Zn adopt a +2 valence state when doped into the CeO_2 (111) surface, and this results in for-mation of two holes on two neighboring oxygen atoms. A charge compensating oxygen vacancy is therefore required to compensate the holes on the oxygen species, and correctly describe the ground state electronic structure of the doped surfaces which are then used as a platform to investigate methane activation on Cu and Zn doped CeO_2 (111) .

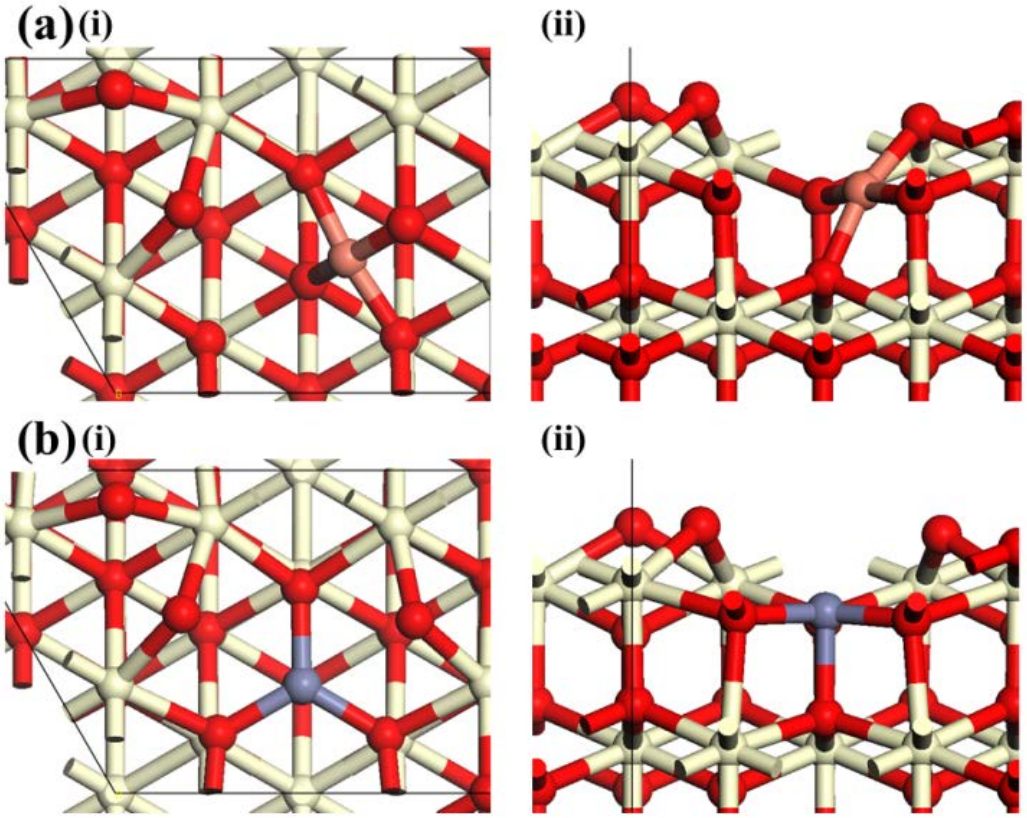


Figure 2: The calculated local structure for (a) Cu and (b) Zn doped CeO_2 (111), along the (i) *c* and (ii) *b* vectors. The red, white, orange and purple spheres are the lattice positions of the O, Ce, Cu and Zn atoms.

3.3 Charge compensating and active oxygen vacancies on Cu and Zn doped CeO_2 (111)

To investigate the charge compensating mechanism on Cu and Zn doped CeO_2, the position of the lattice oxygen atom to be removed relative to the dopant cation is determined by examining all possible oxygen sites relative to the dopant cation, as indicated in Figure 3. These are the two fold nearest neighbor (nn) atoms on the surface layer (surf), the fully coordinated nn oxygen atoms in the sub-surface (sub) layer, the fully coordinate next-nearest neighbor (nnn) oxygen atoms in the surf and sub layers. The surface distortions arising from the inclusion of the dopant cations on the Ce lattice sites, allows

formation of three two-fold surface oxygen atoms that are nn-surf around the dopant, which are expected to be highly active centers for interacting with surface species.

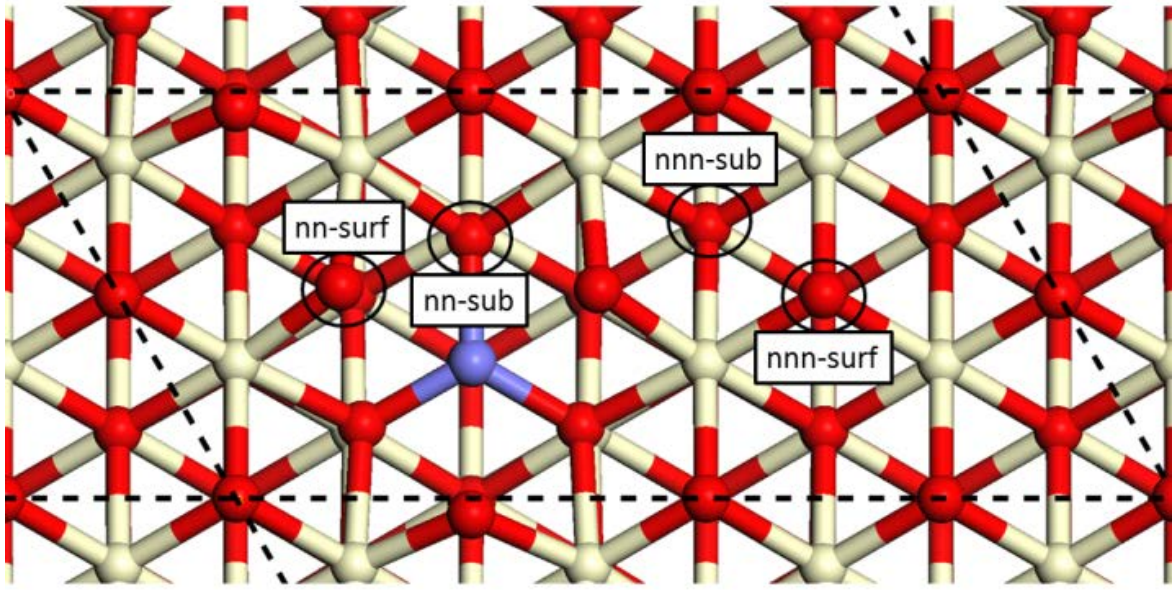


Figure 3: The surface structure of CeO_2 (111) with the dopant site indicated by the purple sphere. The possible sites for the charge compensating vacancy are labelled relative to the dopant lattice position.

The lowest energy configuration for the charge compensated oxygen vacancy in the compensated Cu and Zn doped CeO_2 (111) surface is shown in Figure 4. The preferential position of the vacancy is the nearest neighbor surface (nn-surf) two fold coordinated oxygen atom to the dopant cation on both Cu and Zn doped CeO_2, as indicated by the black sphere in Figure 4. The calculated formation energy for the charge compensating vacancy on Cu and Zn doped CeO_2 is -0.64 eV and -1.63eV, respectively. The negative values for the formation energies indicate that spontaneous formation occurs, so that the +2 dopants are correctly charge compensated. While these energies will depend on the DFT+U setup, we know from studies of other divalent dopants, that the energies from this set up are consistent with hybrid DFT.[55] The removal of the oxygen atom quenches the holes on the neighboring oxygen atoms since no

spin density is observed on them. There is spin density on the Cu dopant because with a d^9 configuration it has one unpaired electron in its highest occupied orbital, irrespective of the DFT description of the Cu 3d states. If a charge compensating oxygen vacancy is not present, the holes on the oxygen atoms formed from the presence of the dopant will be filled by the adsorption of electron donating species, causing over binding and potentially erroneous adsorption energies.

The calculated PEDOS of the lowest energy configuration for the charge compensating oxygen vacancy on Cu and Zn doped CeO_2 (111) is also shown in Figure 4; a comparison between PBE and PBE+U (+U = 7eV) is presented for interested readers in the supporting information. The plots show that for Cu doped CeO_2, Cu *d* states contribute to the top of the VB mixing with the surface CeO_2 states, and the spin up peak observed at 0.2 eV above the CeO_2 VB is the unpaired electron localized on the Cu dopant, while the spin down peak around 3.2 eV is the empty Cu 3*d* states. The effect of the +U correction on the Cu 3d states is to widen the gap between the occupied and empty Cu 3d states, pushing the occupied 3d state to lower energy. For Zn doped CeO_2, the majority of Zn 3*d* states are located at the bottom of the VB with a peak observed around -4.5eV. The main difference in the Cu and Zn 3*d* contributions to the VB is that the Cu states mix over a large energy range from -4.2eV up to 0eV with the majority of CeO_2 states, while the Zn states mix over a much smaller energy range (-4.5eV to -4.2eV) and thus a negligible amount of CeO_2 surface states. The relevance of the concentration of metal 3*d* states in the VB and their position is important for surface adsorbate interactions which will be discussed in subsequent sections. Both plots have no defect peaks in the CeO_2 surface band gap so that the charge compensated vacancy has compensated the oxygen holes.

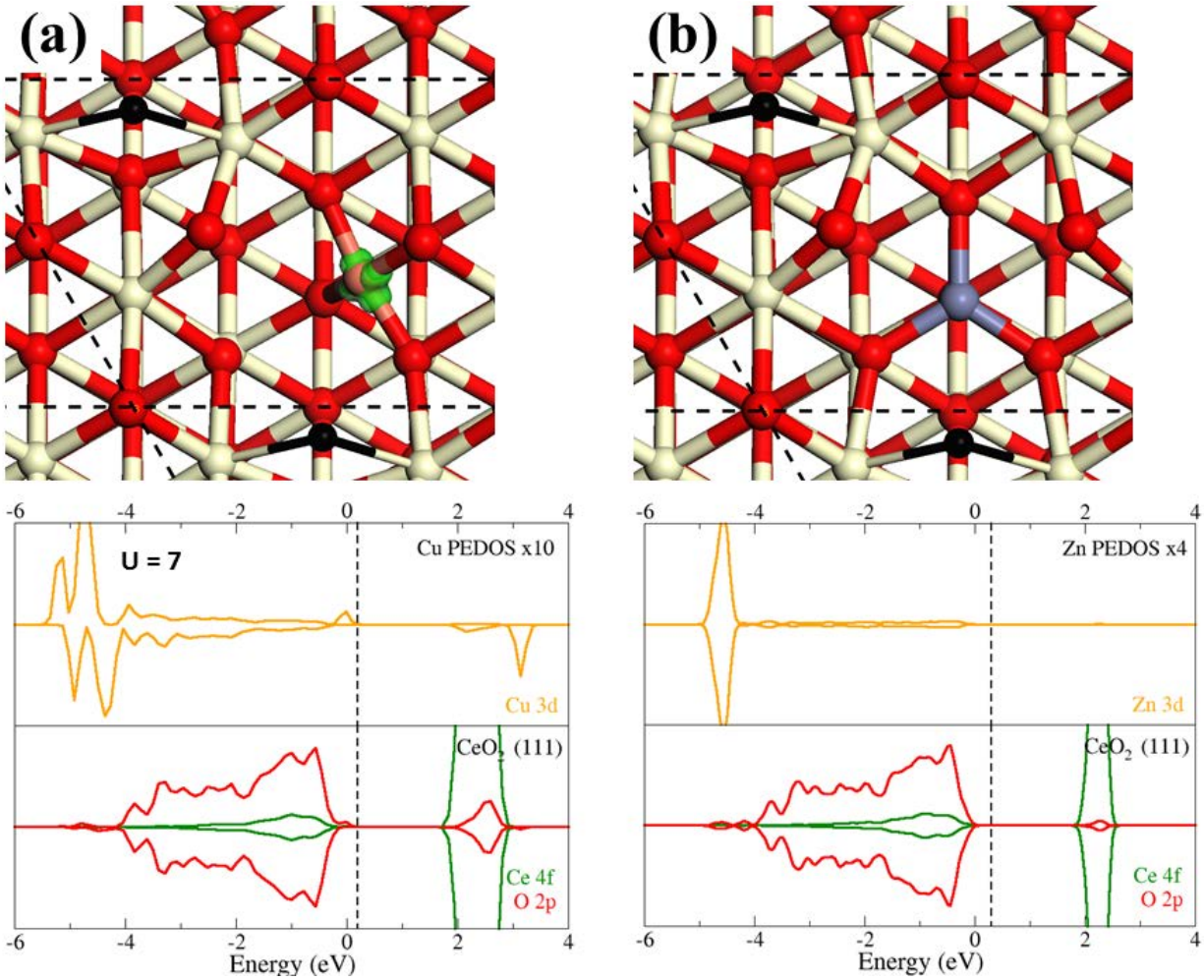


Figure 4: The local geometry for the lowest energy configuration and calculated PEDOS for the charge compensating oxygen vacancy on the (a) Cu (U_{3d} = 7 eV) and (b) Zn doped CeO_2 (111) surface. The black sphere shows the position of the charge compensating vacancy relative to the dopant. The green isosurface (0.15 electrons Å-3) shows the unpaired electron on the Cu dopant. The top of the VB is aligned to 0eV and the Fermi level is indicated by the dotted line.

The removal of a second oxygen atom from the charge compensated structure creates the active oxygen vacancy, and the formation energy for this oxygen vacancy can be compared to the reduced CeO_2 (111) surface. Similar to the investigation of the lowest energy configuration for the charge compensating vacancy, all neighboring oxygen species are examined relative to the dopant to determine the lowest

energy structure to remove a second oxygen atom from the charge compensated surface. The most favorable configuration is the two-fold nn-surf oxygen atom on both Cu (irrespective of DFT approach) and Zn doped surfaces as shown by the blue sphere in Figure 5. The calculated formation energies for the active oxygen vacancy on the doped CeO_2 (111) surface are +0.73 eV Cu doping, with +U correction and +0.67eV for Zn doping. The energies are lower than the formation energy for an oxygen vacancy on the undoped (111) surface indicating that both dopants improve the reducibility and hence the oxygen storage capacity of the CeO_2 (111) surface by a similar amount. Both the compensated vacancy and the active vacancy site on each doped CeO_2 (111) surface are on the surface rather than sub-surface, suggesting that these dopants promote oxygen vacancies on the surface rather than in the sub-surface layers which is important for oxygenation reactions on the surface. The active vacancy site on both doped surfaces is next neighbor oxygen to the compensating vacancy and not bound to the dopant, which creates a distorted surface geometry deprived of surface oxygen, and an unusual 5-coordinated Ce cation on the surface. To adjust for the lack of surface oxygen species, a subsurface oxygen atom migrates to the surface layer becoming three-fold coordinated, as indicated by the orange sphere in Figure 5. The creation of the active oxygen vacancy nearest neighbor to the compensating vacancy from the presence of dopants on the surface causes drastic geometric changes to the surface which may act as defective sites to facilitate surface reactions. Although the removal of surface oxygen species distorts the surface geometry, the local structure around the dopant in the surface is little changed, showing that their bonding configurations are unaffected by the creation of surface vacancies.

The formation of the active oxygen vacancy at the surface releases two electrons that reduce two surface Ce(IV) cations to Ce(III) cations that are shown in Figure 5 by the large green spheres. The spin magnetization shows a value of 1 on the Ce cations in the lattice marked by the green spheres, while the Bader charges show an increase from 9.6 to 9.9 electrons that is typical for the reduction of the Ce cations. For Cu-doped CeO_2 (111) the two reduced Ce cations are neighboring the vacancy on the surface

and the Cu dopant maintains its +2 oxidation state as indicated by the spin density, while for Zn-doped CeO_2 (111) the preferential sites are one surface Ce cation and a sub-surface Ce cation. The reduction of the Ce cations is further shown in the PEDOS plots with the presence of Ce 4*f* defect levels in the band gap. The two peaks in the band gap for Zn-doped CeO_2 (111) correspond to the reduced Ce cations in two different environments, while in Cu-doped CeO_2 (111) a single peak is present due to the symmetry of the two reduced Ce cations. The spin magnetization also confirms that the Cu atom contains an un-paired 3*d* electron, and the creation of the active vacancy provides a quartet electronic ground state with the unpaired Cu 3*d* and two Ce(III) 4*f* electrons. The doublet electronic ground state, in which the spins on Cu(II) and on one Ce(III) cation are spin paired is 0.1eV higher in energy, so the high spin solution is shown. The Zn-doped CeO_2 (111) system is not as complicated as Zn has a $3d^{10}$ configuration with all electrons being spin paired, and thus the overall ground state is a triplet with two unpaired electrons on the reduced Ce(III) cations.

The calculated PEDOS for the active vacancy for both doped surfaces is also shown in Figure 5. The VB is a mixture of Cu/Zn 3*d* states with the CeO_2 O 2*p* states with a minor contribution from the Ce 4*f* states. Similar to the charge compensated structures, the Cu 3*d* states extends over a large energy range (-4.5eV to 0eV) while the majority of Zn 3*d* states are concentrated in one peak around -4.5eV. For Cu doped CeO_2, the occupied spin up peak around 0.2 eV above the VB is the unpaired electron on the Cu dopant, while the spin down around 3.1 eV peak is unoccupied. The appearance of occupied Ce 4*f* states peaks in the band gap for both doped surfaces confirms the presence of reduced Ce cations in the sys-tem. One peak is present for Cu doped CeO_2 as the reduced Ce cations are symmetry equivalent, while for Zn doped CeO_2 there are two Ce 4*f* peaks in the band gap, each one related to a reduced Ce cation in the surface and sub-surface layers. The Ce defect peak closest to the top of the VB corresponds to the surface Ce atom, while the higher energy Ce defect corresponds to the sub-surface Ce atom.

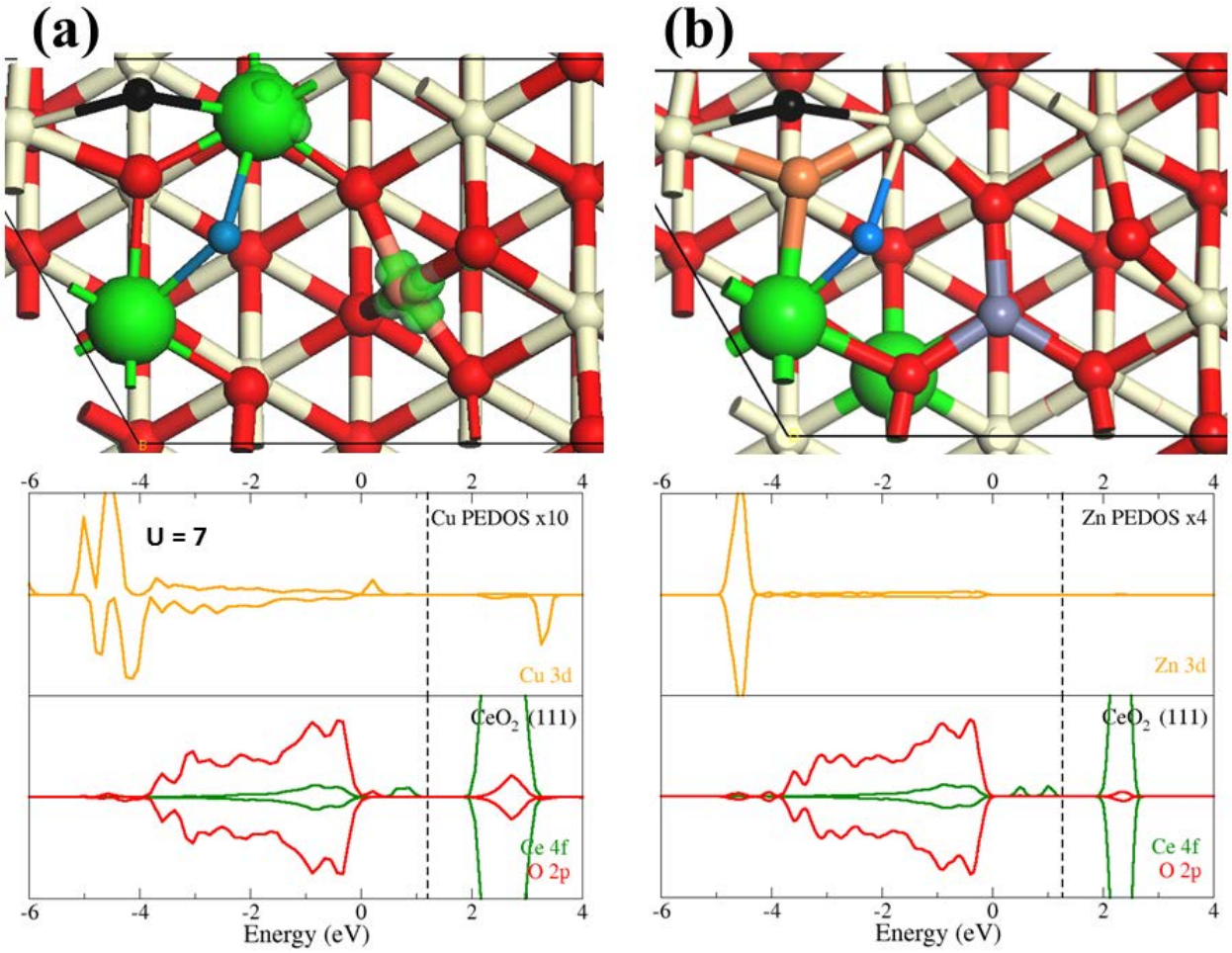


Figure 5: The local structure and calculated PEDOS for the active vacancy formation on (a) Cu (U = 7 eV), and (b) Zn doped CeO_2 (111). The green spheres indicate the lattice positions of the reduced species on both surfaces. The black and blue spheres show the lattice positions of the compensating and active oxygen vacancies, respectively, while the orange sphere indicates the lattice position of a three-fold oxygen species. The red, orange and green lines on the PEDOS plot are the O 2*p*, Cu 3*d*, and Ce 4*f* state contributions to the VB and CB, and the top of the VB is aligned to 0eV and the Fermi level is indicated by the black dotted line on the plot.

3.4 Hydrogen adsorption on Cu and Zn doped CeO_2 (111)

The adsorption of hydrogen was explored on Cu and Zn doped CeO_2 (111) by investigating the interaction of the adsorbate on each of the possible oxygen surface sites labelled in Figure 6. These are identified as the nearest neighbor surface (nn-surf) oxygen, nearest neighbor sub-surface (nn-sub surf) oxygen, oxygen bonded to the dopant (M-O) and the next nearest neighbor surface oxygen atom (nnn-surf) relative to the dopant cation.

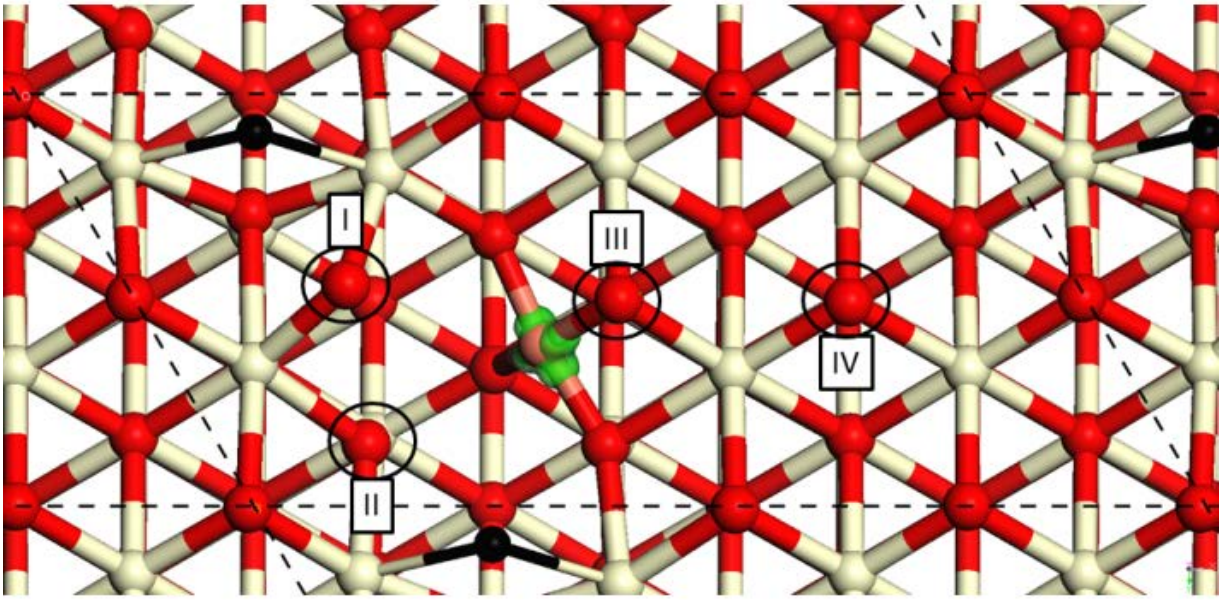


Figure 6: The possible surface oxygen adsorption sites on Cu-doped CeO_2 (111) for exploring hydrogen adsorption are identified as (I) nn-surf, (II) nn-sub surf, (III) M-O and (IV) nnn-surf. The dotted lines indicate the edges of the unit cell surface.

The lowest energy configuration for hydrogen adsorption on Cu and Zn doped CeO_2 (111) is shown in Figure 7. The preferential adsorption site for hydrogen on Cu doped CeO_2 is on nn-surf two-fold coordinated oxygen atom not bound to the dopant. On Zn doped CeO_2 hydrogen also adsorbs on nn-surf two-fold oxygen atom not bound to the Zn dopant. Surface hydroxyls are formed with an O-H bond

length of 0.97Å in each case. The calculated hydrogen adsorption energies on doped CeO_2 are -1.72 eV and -1.68eV (Zn), all relative to 1/2 H_2 in the gas phase, which indicate that the adsorption is favorable on both surfaces. The calculated H adsorption energy on the undoped surface is -1.26eV indicating that the Cu and Zn dopants promote H adsorption on the CeO_2 (111) surface.

The adsorption of hydrogen transfers an electron from the adsorbate to both doped surfaces, reducing a next nearest neighboring Ce(IV) cation to Ce(III), as shown by the large green spheres in Figure 7, and further confirmed by spin magnetization and Bader analysis. The spin magnetization indicates that the Ce cations have a spin of 1 from the unpaired electron, and the Bader values show that the hydrogen atom is a proton while the computed charge on the reduced Ce cations charge is 9.9, confirming the electron transfer process. The spin density plot on the Cu dopant shows that the Cu atom maintains its +2 oxidation state.

The PEDOS for hydrogen adsorption on Cu and Zn doped CeO_2 is shown in Figure 7. The H 1s peak is low in energy around -5eV for both doped surfaces, which mixes with Cu 3d states and close in energy to the large Zn 3d peak (-4.5eV). There is negligible mixing with the CeO_2 surface states. The occupied Cu 3d states are seen to be present across a wide energy range from 0.0eV to -5eV, while for Zn 3d state are mainly located in the peak around -4.5eV. Both PEDOS plots show a Ce 4*f* state in the band gap which is associated with the reduced Ce cation formed by the transfer of an electron from the hydrogen atom.

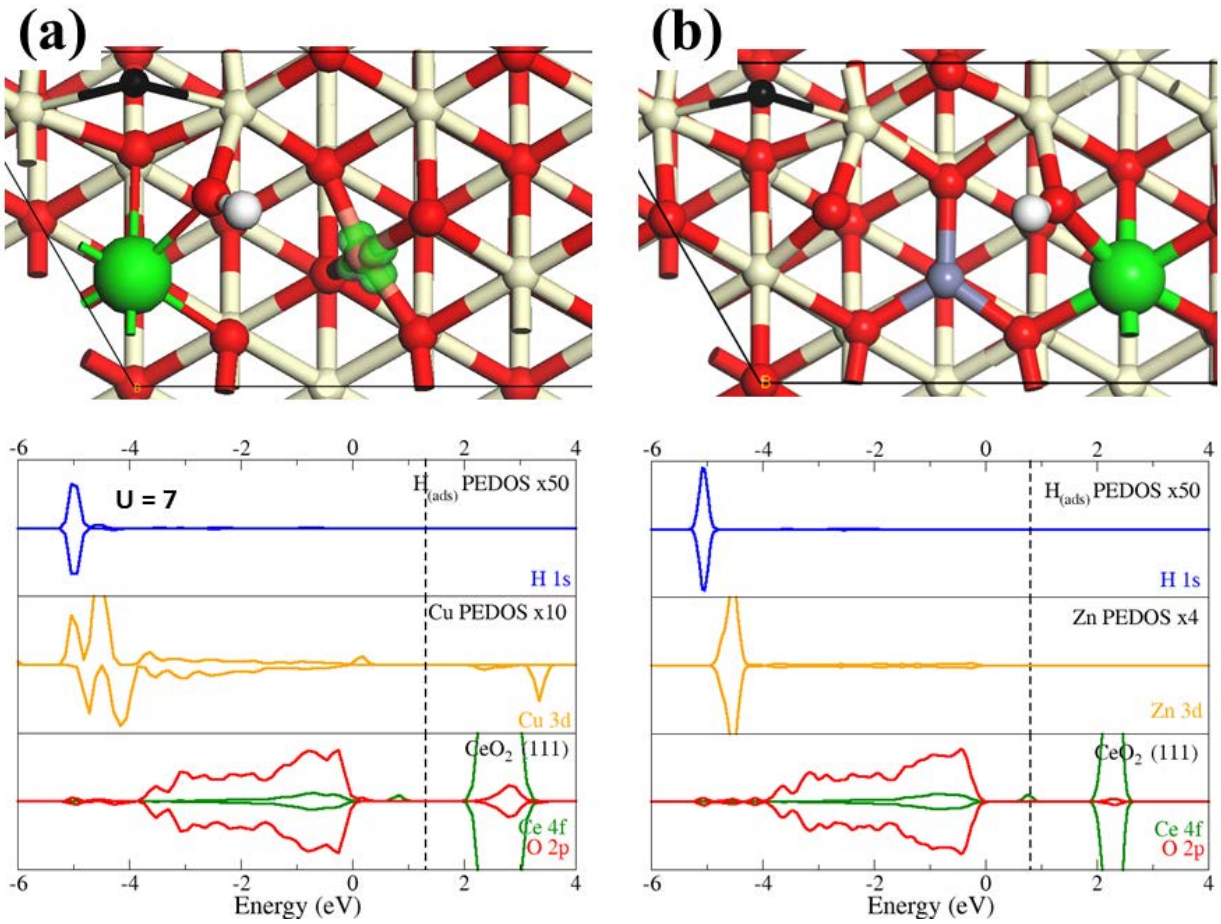


Figure 7: The most stable site and associated PEDOS plot for hydrogen adsorption on (a) Cu (U = 7 eV), and (b) Zn doped CeO_2 (111). The local atomic structure is shown for the H adsorption site with the black sphere indicating the position of the compensated vacancy, and the large green spheres show the lattice positions of the reduced Ce cations, with the green iso-surface (0.15 electrons $Å^{-3}$) showing the spin density on the Cu dopant. The top of the VB is aligned to 0eV and the Fermi level is indicated by the dotted line.

3.5 Dissociative adsorption of methane on Cu and Zn doped CeO_2 (111)

The dissociative adsorption of methane was investigated on Cu and Zn doped CeO_2 (111) by examining possible adsorption structures on the surface in a similar manner to hydrogen adsorption. In all cases methane was found to weakly interact with both doped surfaces in a physisorbed state, lying 3Å above

the surface as shown in top panels in Figures 8 (a) and (b) for Cu and Zn doped CeO_2 (111). This suggests that the CH_4 molecule does not dissociate on interaction with the doped surfaces and the molecule has to be activated to dissociate.

The lowest energy configuration for the CH_3^* + H dissociation products was investigated by determining the lowest energy adsorption site for single adsorption of CH_3* and using the most stable adsorption site for hydrogen adsorption on each surface. The co-adsorption of these two species (CH_3^* + H) was also investigated to explore and contrast the most stable adsorption sites relative to each other, finding that the most stable positions are similar to their single adsorption lowest energy configurations. The same lowest energy structure is also found when CH_3* is adsorbed after H adsorption. The lowest energy configurations for the dissociation products are shown in the lower panels of Figures 8(a) and (b) for the Cu and Zn doped CeO_2 (111). Irrespective of dopant or DFT approach, the H adsorbate prefers to adsorb on the two fold active surface oxygen species next to the dopant cation on both surfaces, and the subsequent adsorption of the CH_3^*species was explored around the lowest energy H site. In all cases, adsorbed CH_3^* prefers to bind to the three-fold coordinated surface oxygen species next neighbor to the Cu dopant, to form a surface methoxy species (CH_3-O). On adsorption of the CH_3* species, the Cu-O bond is broken to accommodate CH_3-O formation, and a two-fold coordinated surface oxygen atom is formed from the three-fold species. This oxygen is bonded to two Ce cations close to the dopant and across from the hydroxyl species. When we examine other adsorption sites for both H and CH_3, particularly in which one or both adsorbates bind to other three-fold coordinated oxygen surface species, the adsorption energies can be up to 1.2 eV higher than those for the structures in Figure 8. Thus, adsorption of H and/or CH_3 is favored at the 2-fold oxygen formed by the presence of the lower valent dopant and compensating oxygen vacancy.

The methoxy species on both surfaces have similar bond lengths; the C-H distances are 1.10Å similar to the CH_4 molecule, the O-C surface bond is 1.42Å and the H-O bond is 0.97Å for adsorbates on both

surfaces. The preferential adsorption of dissociation products occurring at the dopant site indicates that the dissociation of methane is localized around the dopant site. The dopant facilitates the dissociation due to the local structural changes, originating from the charge compensating vacancy being next neighbor on the surface and the creation of the reactive two fold oxygen surface species. The calculated adsorption energies for the dissociated species are -1.54 eV for Cu doped and -2.05eV for Zn doped CeO_2 (111), which are significantly lower in energy than adsorption energy of the CH_3^*+H species on the pure surface (-1.14eV). The negative adsorption energies indicate that adsorption and dissociation is favored on both doped surfaces. The Cu and Zn doping therefore promotes methane dissociation with a thermodynamic drive to form the dissociation products being greater, in particular on Zn-doped CeO_2 (111).

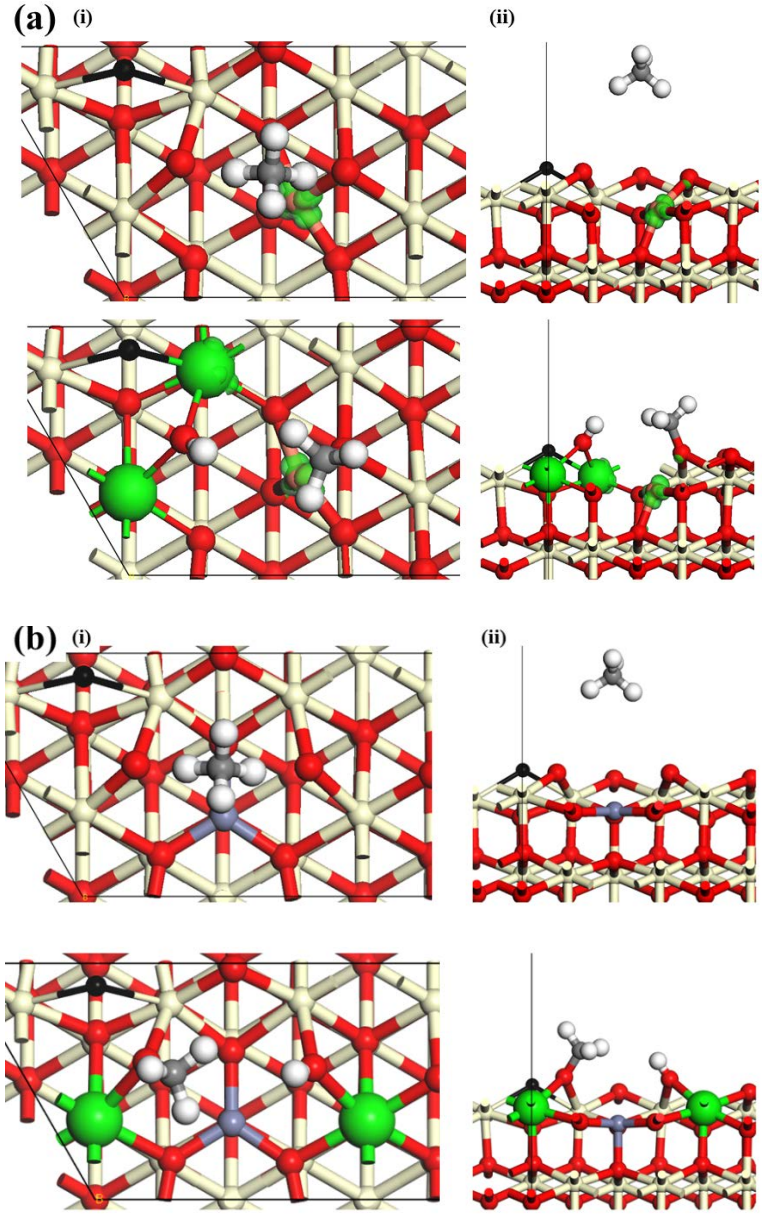


Figure 8: The local atomic structures for the dissociative adsorption of methane on (a) Cu and (b) Zn doped CeO_2 (111) shown along the (i) *c* and (ii) *b* vectors. The top panel shows the lowest energy configuration for CH_4, while the bottom panel shows the lowest energy configuration for CH_3+H on both doped structures. The large green spheres show the location of the reduced Ce cations on the surface.

The calculated ground state electronic structure for the dissociative adsorption of methane on Cu and Zn doped CeO_2 (111) was investigated by spin magnetization, Bader analysis and PEDOS plots which

are shown in Figure 9. As the methane molecule interacts weakly with both doped surfaces, the electronic structures for the surfaces remain unchanged to that seen previously for the compensated structures. This is reflected in the PEDOS plot shown in Figure 9(a)(i), as the C 2*p* and H 1*s* contributions to the CH_4 molecule overlap around -3.2eV indicating a σ-bonding interaction, and the Cu 3*d* states are similar to those for Cu-doped CeO_2. The spin up peak at the VB edge is for the unpaired Cu 3*d* electron which is shown by the green spin density around the Cu dopant. There are no defect peaks in the band gap for CeO_2 (111) suggesting that no surface defects are present. For Zn-doped CeO_2 (111), the interaction of methane is also weak and does not change the surface electronic structure. The PEDOS for CH_4 on the Zn-doped surface shown in Figure 9(b)(i) is similar to CH_4 on the Cu-doped surface. The Zn 3*d* PEDOS is similar to the charge compensated surface (Figure 4(b)), and there are no observable defect peaks in the CeO_2 (111) PEDOS.

On dissociation and adsorption of the CH_3^*+H species, the changes to the electronic structure are seen from the appearance of reduced Ce surface cations (green spheres) and also seen in the PEDOS plots. For Cu-doped CeO_2 (111), the spin magnetization and Bader values indicate that two surface Ce(IV) cations become reduced to Ce(III) cations next to the H adsorbate as shown by the large green spheres in Figure 8, while the Cu dopant maintains a +2 oxidation state as shown by the spin density around the Cu atom. Investigation of the system magnetization confirms that both reduced Ce cations have a spin of one, and the Cu dopant has an unpaired electron with a spin of 1. The Bader values indicate that the H adsorbate loses electron density becoming a proton to reduce one of the Ce surface cations, while the C atom from the methoxy species loses 0.8 electrons, and the Cu dopant does not lose any electron density. The spin magnetization and Bader values suggest that the Ce cations are reduced after adsorption of the CH_3* and H species. The change in the electronic structure for the dissociation products on Zn-doped CeO_2 (111) is not as complicated as Cu-doped CeO_2 (111). The spin magnetization indicates that two surface Ce cations are reduced (both have a spin of one) from the CH_3^* and H adsorbates donating

electron density to the nearest neighbor surface Ce cations that are shown by the large green spheres in Figure 8. The reduction of Ce cations is supported by Bader analysis, with an increase in charge for the Ce cations and a decrease in charge for the CH_3^*, H adsorbates.

The calculated PEDOS plots for the adsorption of CH_3^*+H on Cu and Zn doped CeO_2 (111) are shown in Figure 9(a) and (b) (ii). The contributions from the 3H atoms for the CH_3 adsorbate and the H adsorbate on the surface are presented separately in the PEDOS to show the differences in their electronic structures. The changes to the C 2*p* and H 1*s* PEDOS from CH_4 adsorption to CH_3^*+H dissociation are seen as these states shift to lower energy, upon interaction with the doped surfaces. For the C and H3 PEDOS of the CH_3^* adsorbate, the peak near the top of the VB is the position of an occupied σ-orbital that is present from the formation of the C-O covalent bond in the CH_3-O moiety, and lies higher in energy on the Zn-doped surface, than on the Cu-doped surface. The H 1*s* peak for the H adsorbate on the Zn-doped surface is lower in energy than the corresponding peak on the Cu-doped surface indicating that the H species is more strongly stabilised on Zn-doped CeO_2 than on Cu-doped CeO_2. The stabilization of the dissociation products is reflected in the calculated adsorption energies which is more favorable on Zn doped CeO_2 than Cu-doped CeO_2. This stabilisation may originate from the interaction of a large portion of the Zn 3*d* states with the C 2*p* and H 1*s* states as seen in Figure 9 (b)(ii), while this interaction with the Cu 3*d* states does not occur (Figure 9(a)(ii)). The reduction of the Ce surface cations on both surfaces is reflected in the PEDOS plots from the appearance of Ce 4*f* peaks around 1eV above the VB.

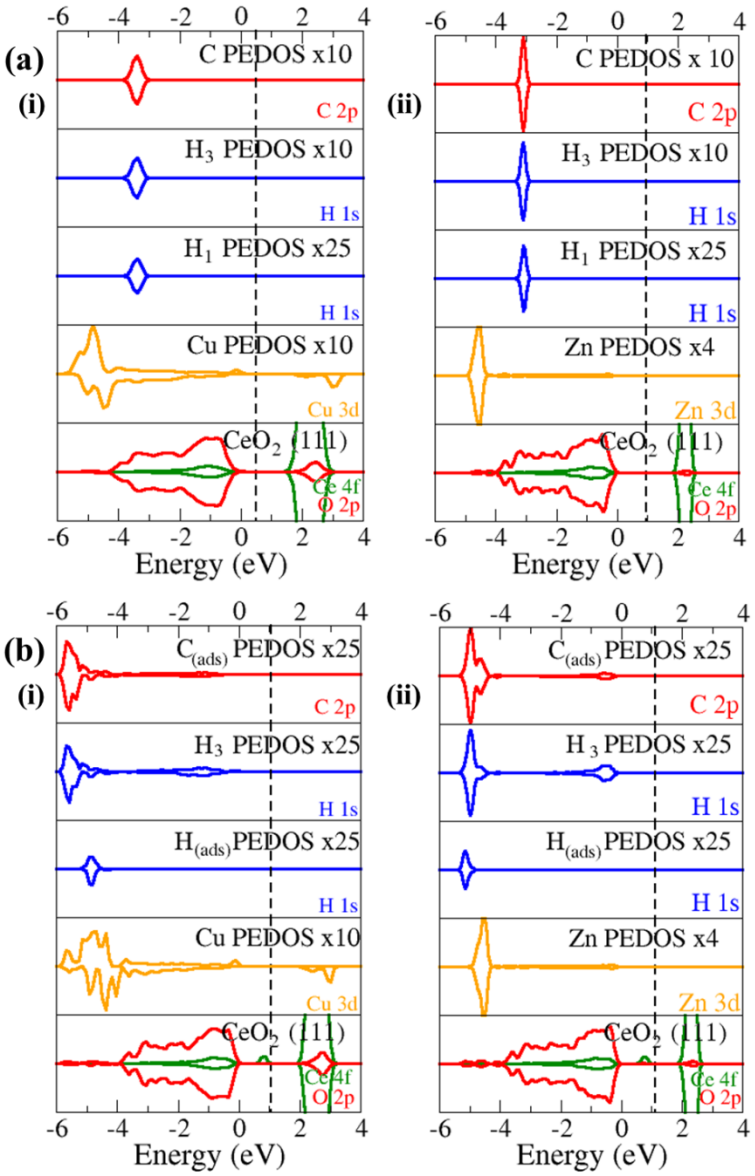


Figure 9: The calculated PEDOS on (a) Cu and (b) Zn- doped CeO_2 (111) for (i) CH_4 and (ii) CH_3 + H. The blue, red, orange and green lines are the *s*, *p*, *d*, and *f* states with the top of the VB aligned to 0eV and the Fermi level is indicated by the dotted line.

3.6 Activation energies for methane dissociation on Cu and Zn doped CeO_2 (111)

The kinetic barriers for CH_4 activation on the Cu and Zn doped CeO_2 (111) surfaces were determined by the CI-NEB method, using the lowest energy configurations for the CH_4 adsorbate and the CH_3*+H dissociation products to anchor the starting and end points of the calculation. The transition state is determined as a maximum point on the potential energy surface between these two points, giving the activation energy to dissociate methane on the doped surfaces. The calculated structures for the transition states on Cu- and Zn-doped CeO_2 (111) surfaces are shown in Figure 10. For both doped surfaces, the transition state shows that the abstraction of an H atom from the CH_4 molecule occurs to form a methyl group (CH_3), and a hydroxyl O-H surface species. On both the Cu-CeO_2 and Zn-CeO_2 surfaces, the methyl group lies in a planar configuration above the surface in the gas phase. The geometry of the methyl radicals for both transition states facilitates the formation of a C-O bond in the final methoxide surface species upon dissociation as the C atom is able to bond with the surface oxygen atoms.

The spin magnetization of the transition state was also determined and supported by Bader analysis. For both Cu and Zn-doped CeO_2, the methyl group remains in the gas phase with an unpaired electron in the σ-SOMO orbital as shown by the iso-surface in Figure 10(b), while upon adsorption of the H atom, an electron is transferred to the neighboring Ce(IV) atom reducing it to Ce(III), which is indicated by the large green sphere. The overall spin for this transition state is a triplet, arising from the unpaired electron on the methyl species, and the reduction of a surface Ce cation by the adsorbed H atom as shown from the spin density plot in Figure 10 (c). The Cu dopant remains in a +2 oxidation state for both the end points and in the transition state structure, which is determined from the Bader charges and calculated spin magnetization. However, this is not reflected in the spin density plot of the transition state as the unpaired electron on the Cu dopant has an opposite spin to the methyl group and Ce(III) cation.

The calculated activation energies on Cu-CeO_2 and Zn-CeO_2 (111) surfaces are 1.23eV and 0.85eV. The energies indicate that the Cu and Zn doping improves the activation of methane on CeO_2 (111) as the computed activation energy is lower than the undoped surface (1.45eV). For Cu-CeO_2, the activation energy is an improvement over the undoped surface, however it is still significantly higher by 0.38eV than for Zn-doped CeO_2, indicating that doping the CeO_2 (111) surface with Zn will enhance methane activation at lower temperatures. There is an additional energy requirement to the activation process on Cu-CeO_2 in order to break the Cu-O bond in the final methoxide state which is an energetically costly step that is not seen for Zn-CeO_2. There is a lengthening of two Cu-O bonds in the transition state in the z-plane, and one of these is broken in the final dissociated state, since the CH_3 adsorbate is bonded to the resulting two fold surface oxygen, Figure 10(a)(iii). The breaking of this Cu-O bond on forming the dissociated adsorption structure adds an extra energy contribution to the activation energy making it higher when compared to the activation energy for Zn-CeO_2. The lower activation energy on Zn-CeO_2 arises from the local geometry around the dopant being little changed during the C-H bond breaking with no Zn-O bonds being broken or formed.

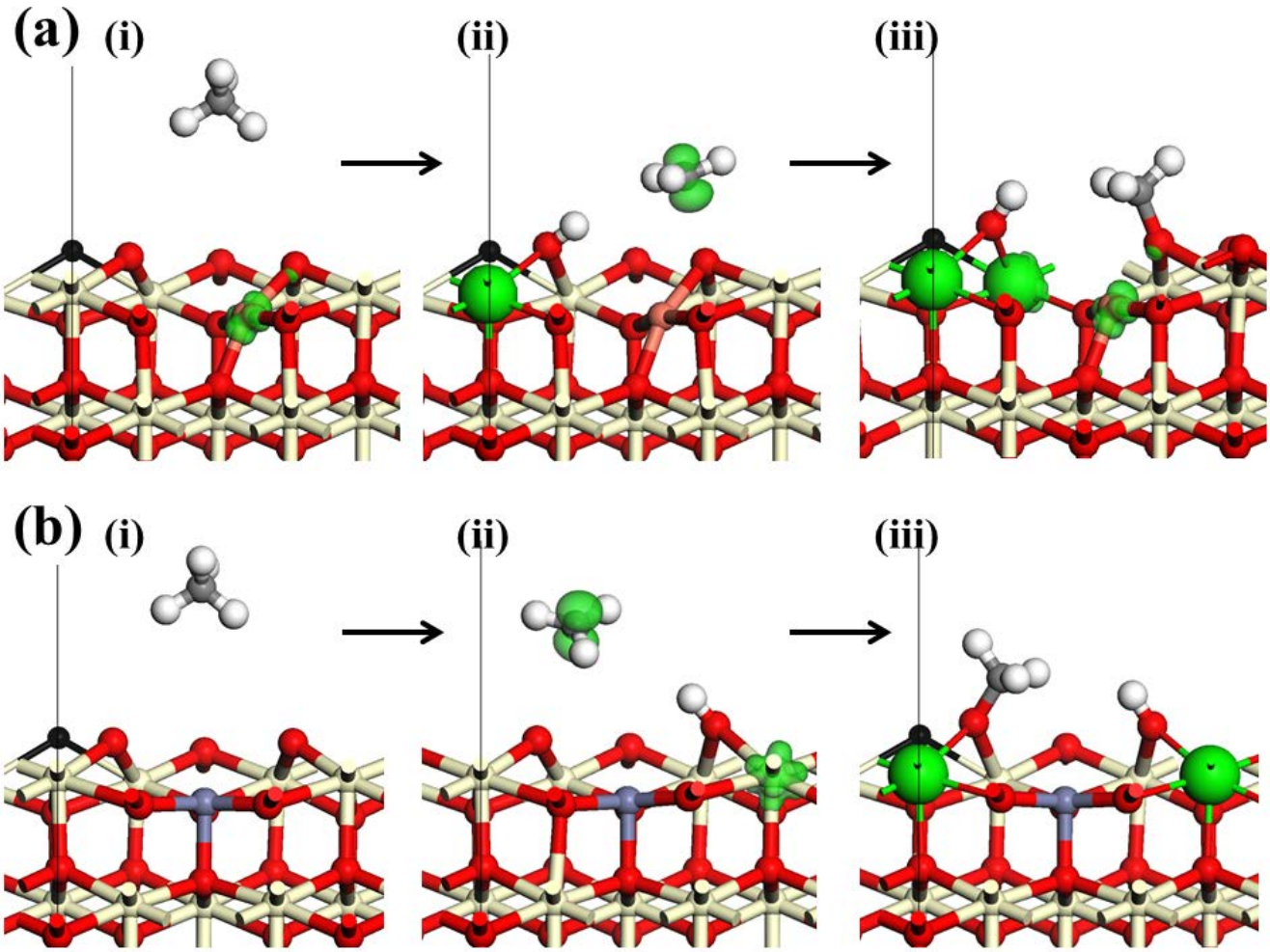


Figure 10: The calculated structures to determine the activation energy on (a) Cu doped CeO_2 (111) with a U=7 correction applied to the Cu 3d states, and (b) Zn doped CeO_2 (111) showing the (i) CH_4 adsorption, (ii) computed transition state and (iii) the dissociated CH_3*+H adsorption products. The large green spheres show the location of the Ce(III) cations, while the green isosurface (0.15 electrons $Å^{-3}$) shows the unpaired electron on Cu dopant and methyl group.

4. Discussion

Charge compensation, active oxygen vacancy formation and dissociative adsorption of methane were explored on Cu and Zn doped CeO_2 (111), finding distinct differences in the behavior of the dopants and some influence of the DFT approach applied to describe Cu 3d states. The negative formation energies for the first oxygen vacancy in the Cu and Zn doping of the CeO_2 (111) surface provides evidence that a charge compensating oxygen vacancy is required to correctly describe the ground state electronic structure of these surfaces,[22] which has been previously neglected in earlier studies of methane activation on doped ceria, e.g. refs.[21, 23] The formation of charge compensating oxygen vacancies in technologically important materials is well-known, e.g. Y-doped ZrO_2 (YSZ, used in fuel cells) and Al-doped TiO_2.[70-72] The removal of a second oxygen atom, that is, the active oxygen vacancy, is endothermic and it is this energy that is compared to the oxygen vacancy formation energy of the undoped CeO_2 (111) surface. Oxygen vacancy formation is enhanced by the presence of the Cu and Zn dopants. We examined the adsorption of H and CH_3+H on the doped surfaces; the calculated adsorption energies are much smaller than calculated for Zn-CeO_2 on the non-compensated structures in previous works.[23] The large binding energies on the non-compensated Zn-CeO_2 (111) surface are not surprising as the adsorbates are electron donating species and over-bind when hole states are present on the surface oxygen atoms. The over-binding of these adsorbates and the use of negative oxygen vacancy formation energies in previous works brings into question the validity of the developed trends, and perhaps a reevaluation is needed.[23] The calculated adsorption energies in this work on the compensated surfaces and the calculated formation energies for the active vacancies are more appropriate since the ground state electronic structure is correctly described and the calculated energies fit better with the energies of higher valence dopants in CeO_2.

The active oxygen vacancy formation energies and the adsorption energy for H on both Cu and Zn doped CeO_2 are similar; however the calculated energy for the adsorption of the CH_3 species on the

surface for the lowest energy configuration of CH_3+H is very different. The co-adsorption of these species on the Zn-CeO_2 (111) surface is greatly stabilized from the single adsorption of H on the surface by 0.37eV which can be attributed to the acid-base interaction.[73,75] The pre-adsorption of the H species is an acid which donates charge to the surface and the subsequent adsorption of CH_3 is greatly stabilized as a base when compared to single adsorption of either H or CH_3. The calculated adsorption energy for CH_3*+H is destabilized by 0.18 eV compared to the adsorption energy of H.

The H adsorbate and Cu dopant act as acids on the surface so that the surface becomes too electron rich to stabilize the subsequent adsorption of the CH_3 species as a base interaction, and results in the weaker, although still favorable, overall adsorption energy. The transition state structure for the Cu-CeO_2 (111) surface is the methyl group in the gas phase above the surface to facilitate the formation of the H_3C-O bond in the final state. Although the structure is similar to Zn-CeO_2, the activation energy is still 0.38eV higher than Zn-CeO_2 indicating that Zn doped CeO_2 will break the C-H bond at lower temperatures than the Cu doped CeO_2 surface. The large energy requirement for Cu-CeO_2 is due to the Cu dopant having a four coordinated square planar geometry when only a H atom is adsorbed, and further adsorption of the CH_3* species breaks the surface Cu-O bond to form a two coordinated O surface species with the methyl group. This is not seen for Zn-CeO_2, as the Zn dopant lies in the sub-surface layer with no surface Zn-O bonds, and therefore there is no additional energy requirements for breaking of M-O bonds to allow adsorption of the final methyl radical.

Low valence, aliovalent and high valence transition metal dopants in metal oxides, as well as the acid-base interaction for adsorbates on their surfaces has been discussed in the literature to predict the properties and reactions that can take place.[73, 74] The comparison of the behavior between the Cu and Zn dopants in this study reveals a further complexity to the interaction and adsorption of atomic and molecular species on transition metal doped CeO_2. The coordination environment of the dopant species plays a role in the reaction thermodynamics and kinetics. Both dopant species are low coordi-

nated as Zn adopts a square pyramidal geometry in the sub surface layer, while Cu has a square planar geometry that bonds with surface oxygen atoms. The Zn dopant coordination geometry facilitates low coordinated surface oxygens as active sites for adsorbate interactions which appear to affect the thermodynamics and kinetics. Careful consideration of the dopant coordination is therefore warranted and must be understood when designing transition metal doped surfaces for different reactions. This may be restricted to transition metal doping in CeO_2 or for methane activation; however further comparisons between dopants with different coordination and for different reaction schemes may support the hypothesis. For this study, the smaller Zn cation is a superior dopant over the Cu dopant as the Zn dopant in the CeO_2 surface enhances the reaction thermodynamics and kinetics over the undoped surface by causing surface distortions to facilitate dissociative adsorption of methane.

5. Conclusion

The formation of oxygen vacancies and dissociative adsorption of methane on Cu and Zn doped CeO_2 (111) surfaces was investigated using density functional theory calculations; in addition, there is a requirement for the +U correction on the 3d states of Cu. The calculations showed that the removal of a first oxygen atom from the divalent doped CeO_2 (111) surface results in a negative formation energy which indicates that a charge compensating mechanism is required to correctly describe the ground state electronic configuration of these doped surfaces, which has been neglected in the current literature. The removal of a second oxygen atom forms the active vacancy. Compared to the oxygen vacancy formation energy of the undoped CeO_2 (111) surface, the Cu and Zn doping enhances oxygen vacancy formation.

The adsorption of H was investigated on the Cu and Zn doped CeO_2 (111) surfaces, and we find that this interaction is more favorable than on the undoped surface. On both doped surfaces, the adsorp-

tion of the H atom reduces one Ce(IV) cation to Ce(III) with no change in the Cu and Zn oxidation states.

Methane is weakly interacting on the Cu and Zn doped surfaces, being phyisorbed around 3Å above the surface. For dissociative adsorption, O-CH_3 and OH surface species are formed. The adsorption of CH_3*+H is more stable on the Zn doped surface than on the Cu doped surface, but both doped surfaces promote dissociative adsorption of methane over the undoped surface. On Zn doped CeO_2 an acid-base interaction gives enhanced stability, while stability of the co-adsorption becomes weaker on Cu-doped CeO_2. This can be related to the activation energies, as Cu-CeO_2 does not lower the dissociation barrier compared to the undoped CeO_2 surface as significantly as Zn-CeO_2, which is proposed to greatly promote dissociation of methane at lower reaction temperatures with faster reaction kinetics. The coordination environment of the dopant plays a leading role in this difference between Cu-CeO_2 and Zn-CeO_2.

6. ACKNOWLEDGMENT

We acknowledge funding from the European FP7 NMP 2013 project BIOGO (grant no: 604296) (Catalytic partial oxidation of biogas and reforming of pyrolysis oil for synthetic gas production and conversion into fuels, www.biogo.eu). Computational resources are provided by the Science Foundation Ireland (SFI) funded Irish Centre for High-end Computing (ICHEC), and by SFI funded resources at Tyndall. We also acknowledge support from COST ACTION CM1104 “Reducible oxides: structure and function”.

7. REFERENCES

1 A. P. York, T. Xiao and M. L. Green, *Topics in Catalysis*, 2003, **22,** 345

2 N. R. Foster, *Applied Catalysis*, 1985, **19,** 1

3 M. J. Brown and N. D. Parkyns, *Catalysis Today*, 1991, **8,** 305

4 N. Abatzoglou and S. Boivin, *Biofuels, Bioproducts and Biorefining*, 2009, **3,** 42

5 S. J. Blanksby and G. B. Ellison, *Accounts of Chemical Research*, 2003, **36,** 255

6 F. Solymosi, A. Erdöhelyi and J. Cserényi, *Catalysis Letters*, 1992, **16,** 399

7 M.-S. Liao and Q.-E. Zhang, *Journal of Molecular Catalysis A: Chemical*, 1998, **136,** 185

8 H. Yang and J. L. Whitten, *The Journal of Chemical Physics*, 1992, **96,** 5529

9 A. Y. Tontegode, *Progress in Surface Science*, 1991, **38,** 201

10 F. Passos, E. Oliveira, L. Mattos and F. Noronha, *Catalysis Letters*, 2006, **110,** 161

11 M. C. J. Bradford and M. A. Vannice, *Catalysis Letters*, 1997, **48,** 31

12 F. B. Passos, E. R. de Oliveira, L. V. Mattos and F. B. Noronha, *Catalysis Today*, 2005, **101,** 23

13 K. Otsuka, Y. Wang, E. Sunada and I. Yamanaka, *Journal of Catalysis*, 1998, **175,** 152

14 V. R. Choudhary, A. M. Rajput and B. Prabhakar, *Catalysis Letters*, 1995, **32,** 391

15 N. M. Kinnunen, J. T. Hirvi, M. Suvanto and T. A. Pakkanen, *The Journal of Physical Chemistry C*, 2011, **115,** 19197

16 S. Wang, G. Q. Lu and G. J. Millar, *Energy & Fuels*, 1996, **10,** 896

17 M. R. Smith and U. S. Ozkan, *Journal of Catalysis*, 1993, **141,** 124

18 K. Otsuka and M. Hatano, *Journal of Catalysis*, 1987, **108,** 252

19 T. J. Hall, J. S. J. Hargreaves, G. J. Hutchings, R. W. Joyner and S. H. Taylor, *Fuel Processing Technology*, 1995, **42,** 151

20 W. Tang, Z. Hu, M. Wang, G. D. Stucky, H. Metiu and E. W. McFarland, *Journal of Catalysis*, 2010, **273,** 125

21 A. D. Mayernick and M. J. Janik, *The Journal of Physical Chemistry C*, 2008, **112,** 14955

22 M. Nolan, Y. Lykhach, N. Tsud, T. Skála, T. Staudt, K. C. Prince, V. Matolín and J. Libuda, *Physical Chemistry Chemical Physics*, 2012, **14,** 1293

23 M. D. Krcha, A. D. Mayernick and M. J. Janik, *Journal of Catalysis*, 2012, **293,** 103

24 A. B. Kehoe, D. O. Scanlon and G. W. Watson, *Chemistry of Materials*, 2011, **23,** 4464

25 V. J. Ferreira, P. Tavares, J. L. Figueiredo and J. L. Faria, *Industrial & Engineering Chemistry Research*, 2012, **51,** 10535

26 Y. Liu, T. Hayakawa, T. Tsunoda, K. Suzuki, S. Hamakawa, K. Murata, R. Shiozaki, T. Ishii and M. Kumagai, *Topics in Catalysis*, 2003, **22,** 205

27 W.-J. Shen, Y. Ichihashi and Y. Matsumura, *Catalysis Letters*, 2002, **79,** 125

28 Z.-Y. Pu, X.-S. Liu, A.-P. Jia, Y.-L. Xie, J.-Q. Lu and M.-F. Luo, *The Journal of Physical Chemistry C*, 2008, **112,** 15045

29 J. Rodriguez, T. Jirsak, A. Freitag, J. Hanson, J. Larese and S. Chaturvedi, *Catalysis Letters*, 1999, **62,** 113

30 X. Qi and M. Flytzani-Stephanopoulos, *Industrial & Engineering Chemistry Research*, 2004, **43,** 3055

31 P. Bera, S. Aruna, K. Patil and M. Hegde, *Journal of Catalysis*, 1999, **186,** 36

32 W.-J. Shen, Y. Ichihashi and Y. Matsumura, *Catalysis Letters*, 2002, **83,** 33

33 T. S. Santos and M. A. Macêdo, *Journal of Superconductivity and Novel Magnetism*, 2013, **26,** 2541

34 A. Penkova, O. H. Laguna, M. A. Centeno and J. A. Odriozola, *The Journal of Physical Chemistry C*, 2012, **116,** 5747

35 N. Iwasa, W. Nomura, T. Mayanagi, S.-i. Fujita, M. Arai and N. Takezawa, *Journal of Chemical Engineering of Japan*, 2004, **37,** 286
36 C. Ledesma and J. Llorca, *The Journal of Physical Chemistry C*, 2011, **115,** 11624
37 J. P. Perdew, K. Burke and M. Ernzerhof, *Physical Review Letters*, 1996, **77,** 3865
38 G. Kresse, *Physical Review B: Condensed Matter*, 1996, **54,** 11
39 G. Kresse and J. Furthmüller, *Computational Materials Science*, 1996, **6,** 15
40 G. Kresse and J. Furthmüller, *Physical Review B*, 1996, **54,** 11169
41 G. Kresse and J. Furthmüller, *Physical Review B: Condensed Matter*, 1996, **54,** 169
42 G. Kresse and D. Joubert, *Physical Review B*, 1999, **59,** 1758
43 M. Nolan, S. Grigoleit, D. C. Sayle, S. C. Parker and G. W. Watson, *Surface Science*, 2005, **576,** 217
44 M. Nolan, S. C. Parker and G. W. Watson, *Surface Science*, 2005, **595,** 223
45 M. Nolan, J. E. Fearon and G. W. Watson, *Solid State Ionics*, 2006, **177,** 3069
46 A. Filippetti and N. A. Spaldin, *Physical Review B*, 2003, **67,** 125109
47 G.-Y. Huang, C.-Y. Wang and J.-T. Wang, *Computer Physics Communications*, 2012, **183,** 1749
48 A. Janotti and C. G. Van de Walle, *physica status solidi (b)*, 2011, **248,** 799
49 E. Chikoidze, M. Nolan, M. Modreanu, V. Sallet and P. Galtier, *Thin Solid Films*, 2008, **516,** 8146
50 M. Nolan and S. D. Elliott, *Physical Chemistry Chemical Physics*, 2006, **8,** 5350
51 A. Filippetti and V. Fiorentini, *Physical Review Letters*, 2005, **95,** 086405
52 X.-Q. Chen, C. L. Fu, C. Franchini and R. Podloucky, *Physical Review B*, 2009, **80,** 094527
53 M. Nolan and G. W. Watson, *Surface Science*, 2005, **586,** 25
54 M. Nolan and G. W. Watson, *The Journal of Chemical Physics*, 2006, **125,** 144701
55 M. Nolan, *Journal of Materials Chemistry*, 2011, **21,** 9160
56 J. J. Carey and M. Nolan, *Catalysis Science & Technology*, 2016, **10.1039/C5CY01787D,**
57 M. Nolan, S. C. Parker and G. W. Watson, *Physical Chemistry Chemical Physics*, 2006, **8,** 216
58 B. G. Johnson, P. M. Gill and J. A. Pople, *The Journal of Chemical Physics*, 1993, **98,** 5612
59 L. A. Curtiss, K. Raghavachari, P. C. Redfern and J. A. Pople, *The Journal of Chemical Physics*, 1997, **106,** 1063
60 B. Hammer, L. B. Hansen and J. K. Nørskov, *Physical Review B*, 1999, **59,** 7413
61 G. Henkelman, A. Arnaldsson and H. Jónsson, *Computational Materials Science*, 2006, **36,** 354
62 E. Sanville, S. D. Kenny, R. Smith and G. Henkelman, *Journal of computational chemistry*, 2007, **28,** 899
63 W. Tang, E. Sanville and G. Henkelman, *Journal of Physics: Condensed Matter*, 2009, **21,** 084204
64 G. Henkelman, G. Jóhannesson and H. Jónsson, *Theoretical Methods in Condensed Phase Chemistry*, 2002, **5**, S. Schwartz, Springer Netherlands, 269
65 G. Henkelman, B. P. Uberuaga and H. Jónsson, *The Journal of Chemical Physics*, 2000, **113,** 9901
66 M. V. Ganduglia-Pirovano, J. L. F. Da Silva and J. Sauer, *Physical Review Letters*, 2009, **102,** 026101
67 G. E. Murgida and M. V. Ganduglia-Pirovano, *Physical Review Letters*, 2013, **110,** 246101
68 Y. Pan, N. Nilius, H.-J. Freund, J. Paier, C. Penschke and J. Sauer, *Physical Review Letters*, 2013, **111,** 206101
69 C. E. Housecroft and A. G. Sharpe, *Inorganic Chemistry*-United Kingdom, 2005, 4th Edition, Pearson Prentice Hall,
70 U. Gesenhues, *Solid State Ionics*, 1997, **101,** 1171
71 U. Gesenhues and T. Rentschler, *Journal of Solid State Chemistry*, 1999, **143,** 210
72 A. Nakamura and J. B. Wagner, *Journal of the Electrochemical Society*, 1986, **133,** 1542
73 H. Metiu, S. Chrétien, Z. Hu, B. Li and X. Sun, *The Journal of Physical Chemistry C*, 2012, **116,** 10439